Rapid semi-quantitative identification of greigite in lacustrine sediments using SIRM/χ and χ_{ARM}: Insights from the Cuo E core, Tibetan Plateau, China

Shengchang Ding [a, b, c, d], Mark J. Dekkers [e], Mingkun Li [f], Qi Zhao [a, b, c], Yi Yan [a, b, c, *], Zhaoyu Zhu [a, b, c, **]

[a] *State Key Laboratory of Isotope Geochemistry, Guangzhou Institute of Geochemistry, Chinese Academy of Sciences, Guangzhou 510640, China*

[b] *CAS Center for Excellence in Deep Earth Science, Guangzhou, 510640, China*

[c] *CAS Key Laboratory of Ocean and Marginal Sea Geology, Guangzhou Institute of Geochemistry, Chinese Academy of Sciences, Guangzhou* 510640, *China*

[d] *College of Earth and Planetary Sciences, University of Chinese Academy of Sciences, Beijing, 100049, China*

[e] *Department of Earth Sciences, Paleomagnetic Laboratory Fort Hoofddijk, Utrecht University, Utrecht, Netherlands*

[f] *School of Geography, South China Normal University, Guangzhou, 510631, China*

ABSTRACT The Cuo E (CE) core contains the entire Quaternary stratigraphy of the Cuo E Lake (31°24′ - 31°.32′ N, 91°28′ - 91°33′E, Tibetan Plateau, China). Here, we study the magnetic properties of 1748 samples from the CE core, combined with scanning electron microscopy and X-ray energy dispersive spectrometer analysis on selected samples. The main magnetic minerals appear to be magnetite and greigite. To further quantify the presence of greigite in CE core, 84 samples were rock magnetically analyzed in more detail including: susceptibility (χ) vs. temperature, coercivity component analysis of acquisition curves of the isothermal remanent magnetization (IRM), and Principal component analysis (PCA) of the first-order reversal curve (FORC) diagrams.

The greigite content and saturation IRM over susceptibility (SIRM/χ) appear to be exponentially related. SIRM/χ can be used as greigite concentration indicator. We also propose a rapid way to identify greigite in the CE core: When the SIRM/χ value increases and anhysteretic remanent susceptibility (χ_{ARM}) increases only slowly, the sample contains greigite. Samples with SIRM/χ < 15kAm^{-1} also obey this relation. This method has a lower limit of detection than the traditionally used SIRM/χ parameter for greigite detection. It is also faster than FORC analysis and thus particularly suitable for analysis of large sample collections. Twenty greigite-bearing layers were identified in the CE core using this method. The location of the Jaramillo subchron in the CE core is controversial in the currently available magnetostratigraphy, possibly related to the presence of greigite in this core interval.

Plain Language Summary Paleomagnetic chronology is an important geological

dating tool for sediment cores or sections that span sufficient duration, and one of its prerequisite is the identification of magnetic minerals. Greigite is a magnetic mineral that may acquire its natural remanent magnetization (NRM) at any time during diagenesis, so it can affect the accuracy of magnetic stratigraphy. In this work, we used rock magnetic methods to identify the main minerals in the Cuo E (CE) core on the Qinghai Tibet Plateau, which are magnetite and greigite. We have also semi-quantitatively expressed the greigite and proposed a rapid semi-quantitative identification method for greigite. This method is faster and simpler than rock magnetic methods and thus particularly suitable for analysis of large sample collections. It can also provide some reference for the research of greigite and magnetic stratigraphy.

Key points:

A rapid method to identify greigite is proposed, which is also applicable to samples with low SIRM/χ

SIRM/χ can be used as greigite concentration indicator and not only to indicate greigite above a certain threshold

20 layers of greigite were identified in the Cuo E core, which may be the cause of inaccurate magnetic stratigraphy

1. Introduction

Lacustrine sediments represent a continuous and high-resolution paleoenvironmental archive, essential for understanding past global and regional environmental change. The dominant magnetic minerals in lacustrine sediments (*i.e.*, magnetite (Fe_3O_4), hematite (αFe_2O_3), and greigite (Fe_3S_4)) reflect different aspects of geological and climatic processes, so lake sediment magnetic properties can be used to reconstruct paleoclimatic information [*C Fu et al.*, 2015; *Peck and King*, 1996; *Peck et al.*, 1994]. Magnetic measurements are important paleoclimate proxies in lacustrine sediments because of their high sensitivity, rapidity, and non-destructive nature [*Q Liu et al.*, 2012]. In addition, for sediment cores or sections that span sufficient duration, magnetostratigraphy is an important dating tool [*Tauxe et al.*, 2010]. The magnetic mineralogy of the sample collection should be known for a proper assessment of the magnetostratigraphic information.

Greigite (Fe_3S_4) is an inverse spinel and a collinear ferrimagnet with antiferromagnetic coupling between iron in octahedral and tetrahedral sites [*Roberts et al.*, 2011a]. It was first reported in 1964 in Miocene lacustrine sediments from San Bernardino County (California, USA) [*Skinner et al.*, 1964]. In the past few decades, greigite has been widely reported as an authigenic ferrimagnetic sulfide in marine and lake environments, such as Heqing paleolake Basin [*Qiang et al.*, 2018], Black Sea [*Neretin et al.*, 2004], Baltic Sea [*Reinholdsson et al.*, 2013], Lake Lop Nur [*W Li et al.*, 2019], Gulf of Mexico [*Y Fu et al.*, 2008], *etc.* Greigite contains important

paleoclimatic information [*Babinszki et al.*, 2007; *Duan et al.*, 2017; *J Liu et al.*, 2021], because it represents a humid and reduced environment. It typically produces gyroremanent magnetization (GRM) during alternating field demagnetization [*Fabio Florindo et al.*, 2003; *Frank et al.*, 2007; *Hu et al.*, 2002a; *Hu et al.*, 1998; *Hu et al.*, 2002b], undergoes thermal alteration during thermal demagnetization [*Porreca et al.*, 2009; *Roberts et al.*, 2011a; *Rowan and Roberts*, 2008], and may acquire its natural remanent magnetization (NRM) at any time during diagenesis [*Roberts and Weaver*, 2005; *Rowan and Roberts*, 2006; *Leonardo Sagnotti et al.*, 2010; *Leonardo Sagnotti et al.*, 2004], which will affect the accuracy of magnetic stratigraphy [*Roberts et al.*, 2011a; *Roberts et al.*, 2010; *Roberts and Weaver*, 2005; *Leonardo Sagnotti et al.*, 2010]. Therefore, it is essential to document the presence of greigite.

Most natural geological samples are mixtures of various magnetic minerals. Therefore, quantifying magnetic minerals in rocks and sediments is an essential, albeit difficult task. At present, the main quantitative methods of magnetic minerals include the principal component analysis (PCA) of first-order reversal curves diagrams (FORC diagrams) [*Harrison et al.*, 2018; *Lascu et al.*, 2015; *Roberts et al.*, 2018; *Wang et al.*, 2020], the extraction of the central ridge in FORC diagrams [*Ramon Egli et al.*, 2010; *Heslop et al.*, 2014], and various forward basis function fitting approaches to isothermal remanent magnetization (IRM) acquisition curves (cumulative log-Gaussian analysis model (CLG), skewed generalized Gaussian fitting) [*Duan et al.*, 2017; *Heslop*, 2015; *Heslop and Dillon*, 2007; *Just et al.*, 2012; *M Li et al.*, 2018; *Roberts et al.*, 2011b].

In this work, we subject the Cuo E (CE) core samples of Qinghai Tibet Plateau to a systematic magnetic property investigation, combined with scanning electron microscopy (SEM) and energy dispersive spectrometer (EDS) X-ray analysis. The main magnetic minerals in the CE core appear to be magnetite and greigite. We used FORC-PCA and IRM acquisition curve fitting to quantify greigite. Based on the relationship between the contribution of greigite and saturation IRM over susceptibility (SIRM/χ) and anhysteretic remanent susceptibility (χ_{ARM}), we propose a method to rapidly quantify greigite. Twenty greigite-bearing layers appear to be present in the CE core. The quantitative method to detect greigite can be used elsewhere for paleomagnetic and environmental magnetic purposes. Previous work on the magnetostratigraphic age model for the CE core, yielded two options: primarily the location of the Jaramillo subchron appears to be equivocal [*Jin et al.*, 2011; *Jin et al.*, 2009; *Shen et al.*, 2004]. The method outlined here also provides a basis to assess the veracity of the magnetostratigraphic framework in the CE core.

2. Materials and methods

2.1. Sampling

Lake CE is located at 31°24′ - 31°.32′ N, 91°28′ - 91°33′E about 200 km north of Lhasa (Tibet Autonomous Region of China) (Fig. 1). Its areal extent is 82.44 km^2 at an elevation of 4519 m [*Zhang et al.*, 2021]; the lake is fed by 14 seasonal rivers. It is

a Na-Cl-HCO_3 brackish lake with a salinity of 12.06 g/L [*Wu et al.*, 2010]. The upper parts of the CE lake Basin are composed of Quaternary lake sediments, and the bedrock underneath is composed of purplish red Cretaceous sandstone and Yanshanian granite. The sediments that occur around the lake basin are mainly Middle Jurassic, Middle-Upper Jurassic, Upper Cretaceous, and Quaternary. The main magmatic rocks in the lake area include the Yanshanian granite, diabase, and ultrabasic rocks, as well as ophiolite of unknown age. Two sets of reverse faults delineate the periphery of the lake basin: a nearly east-west oriented set and a northwest-southeast oriented set. They offset the middle-late Jurassic and late Cretaceous strata and the Yanshannian granite (Fig. 1).

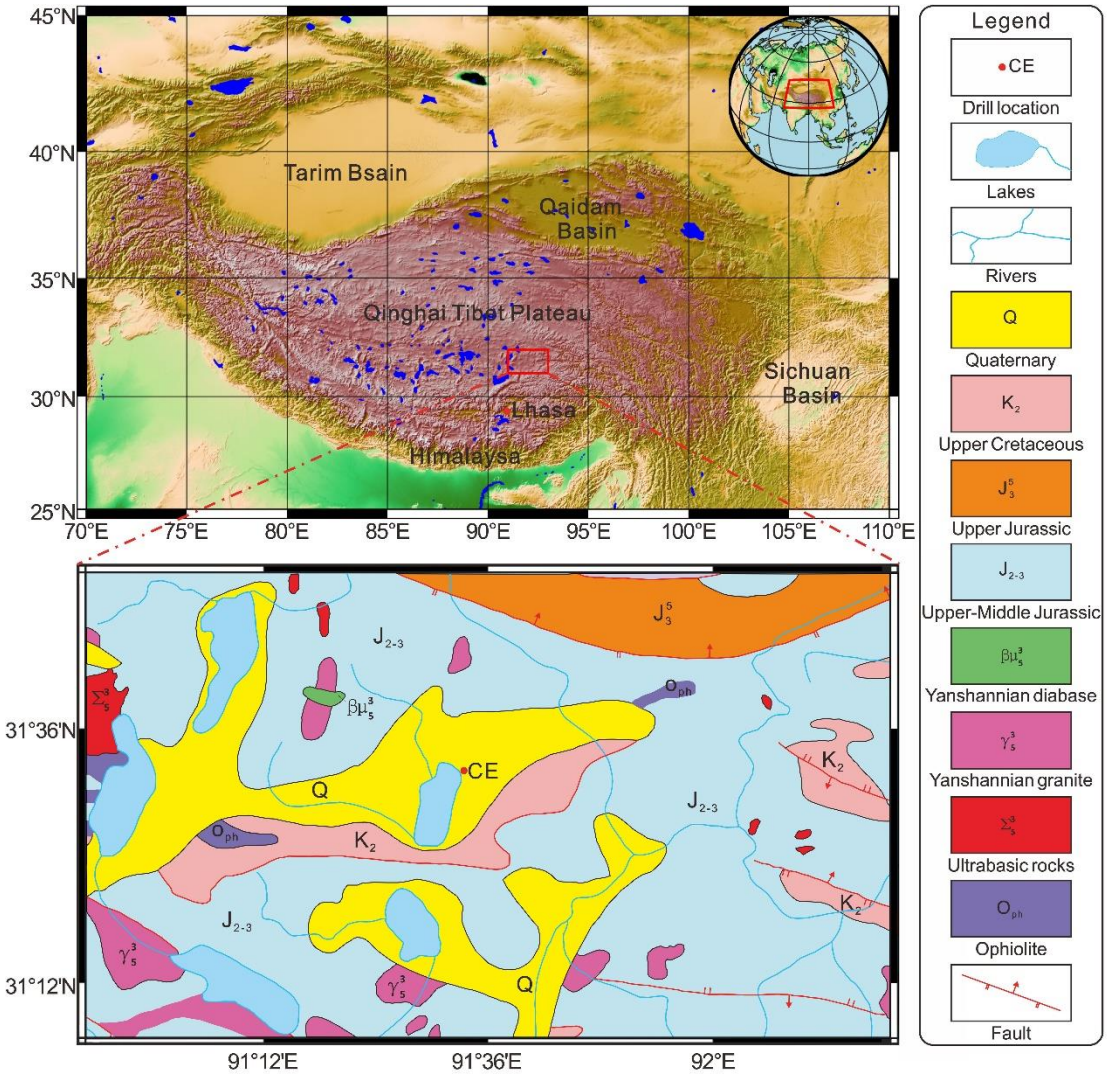

Figure 1. Geographical location and topographical map of the Qinghai Tibetan Plateau (top) and simplified geological map around the Lake CE area (bottom). The inserted globe shows the position of the Qinghai Tibetan Plateau. The geological map shows major geological units, faults, and today's major rivers and lakes.

In July 1999, a 206.5 m-long core was drilled on the eastern swamp side of the Lake CE (Fig. 1), with a core recovery rate of 80% [*Jin et al.*, 2011; *Jin et al.*, 2009]. According to the lithology, the CE core was divided into five units as follows (Fig. 2).

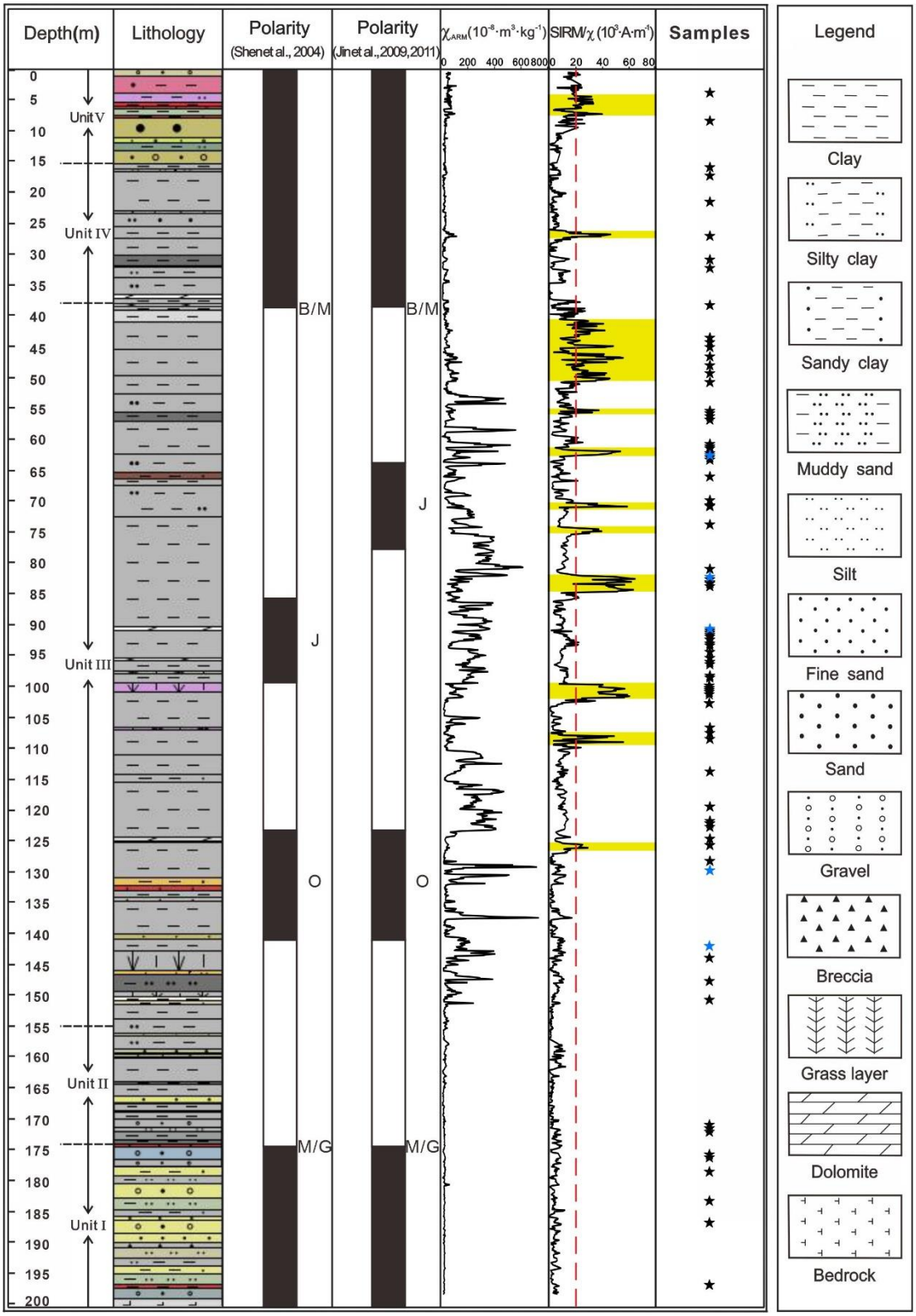

Figure 2. Detailed stratigraphic column of the CE core. Four black dashed lines divide the core into five units. Lithology is plotted using software RESFORM; color represents the color of the sediment. Two controversial paleomagnetic polarity columns and the variation of χ_{ARM} and SIRM/χ as a function of depth are displayed. The red dashed line indicates a value of 20 kA/m for SIRM/χ. Levels marked with yellow horizontal bars have SIRM/χ values > 20 kA/m, indicating the presence of greigite. 84 levels for detailed rock magnetic measurements are marked with stars,

five of which marked with blue stars are considered typical samples to display the rock magnetic results. B/M: Brunhes/Matuyama boundary, J: Jaramillo subchron, O: Olduvai subchron, M/G: Matuyama/Gauss boundary.

Unit I (below 174.35 m) is mainly composed of yellow sand, and contains gravel locally, possibly originating from the underlying Pliocene sediments. The underlying bedrock is visible at 199 m. Unit II (174.35-155 m) is mainly composed of light gray clay mixed with some yellow sand and Fine sand. Units I and II represent the embryonic formation stage of Lake CE. Unit III (155-38.25m) is fine-grained, mainly composed of light gray clay, mixed with minor silty clay; some layers contain many shells (possibly Ostracods) [*Jin et al.*, 2011; *Jin et al.*, 2009]. The intervals 150-143 m and 101-99 m contain significant amounts of peat grass. Three dolomite levels occur in the core at 38.3-38.56 m, 90.64-95.87 m and 124.77-124.97 m. Unit III represents the filling stage in the evolution of Lake CE. Unit IV (38.25-15.63m) mainly consists of gray clay and silty clay mixed with some yellow sand. Unit V (above 15.63m) consists of coarse-grained yellow brown and reddish brown gravel mixed with some yellow sand. Units IV and V represent the gradual cessation of Lake CE's existence [*Shen et al.*, 2004].

The B/M boundary, Olduvai subchron and M/G boundary are unambiguous in the magnetostratigraphic age model of the CE core, but the location of the Jaramillo subchron is ambiguous: two options have been proposed (Fig. 2) [*Jin et al.*, 2011; *Jin et al.*, 2009; *Shen et al.*, 2004]. The lack of a proper identification of the magnetic mineralogy may be the reason for this discrepancy.

2.2. Magnetic measurements

A total of 1748 subsamples (air dried) were taken at an average spacing of 10 cm for magnetic measurement and packed into 2*2*2 cm non-magnetic plastic boxes. Low frequency susceptibility (χ, 976 Hz) was measured with a MFK2-FA Multi-Function Kappabridge instrument (AGICO, Brno, Czech Republic) in the School of Geography, South China Normal University (SGSCNU), Guangzhou, China. Then, anhysteretic remanent magnetization (ARM) and isothermal remanent magnetization at 2000 mT (IRM_{2000mT}) were measured with a Spinner Magnetometer JR-6A instrument (AGICO, Brno, Czech Republic); the corresponding remanences were imparted with an alternating field (AF) Demagnetizer D2000 and an Impulse magnetizer IM-10-30 (ASC Scientific, Santa Barbara, California, USA). The peak AF and direct current (DC) bias field of the ARM are 100 mT and 0.05 mT respectively. The measurements were carried out at the Guangzhou Institute of Geochemistry, Chinese Academy of Sciences (GIGCAS). IRM_{2000mT} is defined as saturation isothermal remanent magnetization (SIRM), and anhysteretic remanent susceptibility (χ_{ARM}), χ_{ARM}/SIRM and SIRM/χ were calculated [*Q Liu et al.*, 2012].

84 samples were selected for more detailed rock magnetic measurements based on their SIRM/χ values (Fig. 2). The hysteresis loops, IRM acquisition curves, backfield demagnetization curves and first-order reversal curves (FORCs) were measured using a VSM8604 vibrating sample magnetometer (VSM) (Lake Shore, Columbus, Ohio,

USA) at the SGSCNU. The magnetic field ranges of the hysteresis loop measurements, IRM acquisition curves and backfield demagnetization curves are -1 T to 1 T, 0 T to 1.5 T and -0.2 T to 0 T, respectively. The high field slope correction parameter is 70%. Saturation magnetization (Ms), saturation remanence (Mrs) and coercive force (Bc) were obtained from the hysteresis loops, and coercivity of remanence (Bcr) was obtained from backfield demagnetization curves. The maximum applied field in the FORC measurement procedure is 1 T, and the field step size is 2 mT. Each FORC diagram contains 200 first-order-reversal curves.

We used the IRM-CLG 1.0 workbook [*Kruiver et al.*, 2001] to fit the IRM acquisition curves (mass specific values enabled between-sample comparison). 84 samples were processed; the 89 data points of each IRM acquisition curve were five-point smoothed and the Gradient Acquisition Plot (GAP) was at the core of the fitting. According to the number of peaks, the field at which half of SIRM is reached ($B_{1/2}$) from the GAP, we can determine the number of components and the average coercive force of each component. Next, the type of magnetic mineral can be determined by the value of dispersion parameter (DP) from the GAP and average coercive force. Finally, based on the peak area proportion of each magnetic mineral, we can obtain the absolute contribution proportion of each magnetic mineral [*R. Egli*, 2004a; b; *Heslop et al.*, 2002; *Robertson and France*, 1994].

The FORC diagrams were generated using FORCinel3.0 [*Harrison and Feinberg*, 2008]. Afterwards, we used FORC-PCA to quantify greigite [*Harrison et al.*, 2018; *Lascu et al.*, 2015]. The process is to first use the FORCinel3.0 program to set VARIFORC smoothing parameters to Sc0 = 10, Sc1 = 3, Sb0 = 10, Sb1 = 3, $\lambda_c = \lambda_b$ = 0.1, and generate the FORC diagram. The same VARIFORC smoothing parameters ensure that results for end members (EMs) and individual samples are comparable [*Roberts et al.*, 2018]. Afterwards, run the PCA Analysis Panel and set the parameters as H_u between -0.1 and 0.1 T, H_c between 0 and 0.12 T, sampling rate of 0.001, and the range of PC1 and PC2 is $-8*10^4$ to $8*10^4$. Finally, set the EMs and define magnetic mineral types, and calculate the absolute content of magnetic minerals in each sample based the on the distance from each sample point to the EMs [*Harrison et al.*, 2018; *Lascu et al.*, 2015].

The thermomagnetic curves (χ-T curves) of the 84 samples were measured with a MFK1-FA Multi-Function susceptometer and a CS4 high temperature furnace apparatus (AGICO, Brno, Czech Republic) at the GIGCAS. The temperature range was set 40–700 °C, and the heating rate was 11.5 °C/min. To prevent sample oxidation, the heating is done in argon.

2.3 Scanning electron microscope observations of the magnetic mineralogy

Magnetic minerals of four samples (CE-0718, CE-0805, CE-0966 and CE-1195) were concentrated by magnetic separation. The morphology and composition of the magnetic minerals were analyzed by backscattered electron (BSE) images obtained with a MIRA 3 scanning electron microscope (SEM) (TESCAN, Brno, Czech Republic) and an element energy dispersive X-ray spectrometer (EDS) (AMETEK

EDAX, Philadelphia, USA) at the Guangzhou Tuoyan Testing Technology Co., Ltd. (China). The operating mode is high vacuum mode, and the accelerating voltage is 20 kV.

3. Results

3.1. Magnetic property analysis

The variation of the magnetic parameters χ, SIRM, and SIRM/χ with depth is plotted on figure 2. Layers marked in yellow, mainly in the light gray clay lithology, have SIRM/χ values higher than 20 kA/m (Fig. 2), indicating the likely presence of iron sulfide [*Roberts*, 1995; *Roberts and Turner*, 1993; *I Snowball and Thompson*, 1998]. We selected five samples to show FORC diagrams, hysteresis loops, χ-T curves, and the Gradient Acquisition Plot (GAP) of the IRM-CLG fits (Fig. 3). Two samples (CE-0671, CE-0805) have higher SIRM/χ values higher than 20 kA/m; they are in the yellow bars (Fig. 2). Three other samples (CE-0880, CE-1210, CE-1319) come from levels with SIRM/χ values lower than 20 kA/m.

3.1.1. FORC diagrams

The FORC diagrams (Fig. 3a-e) show two types of magnetic minerals in the core. CE-0805 has closed concentric contours with B_c peaking at 60-70 mT, which is typical of single domain (SD) greigite [*F. Florindo et al.*, 2007; *J Liu et al.*, 2021; *Roberts et al.*, 2010; *Roberts et al.*, 2006; *Roberts et al.*, 2000]. The FORC diagram of CE-0880 with a B_c peak of 10-20 mT indicates that the magnetic mineral is SD magnetite, while CE-1210 is vortex magnetite with a B_c peak of 20-30 mT [*Roberts et al.*, 2018]. CE-0671 and CE-1319 have two B_c maxima, which indicate that they are mixtures of SD greigite and vortex magnetite, and SD magnetite and vortex magnetite respectively.

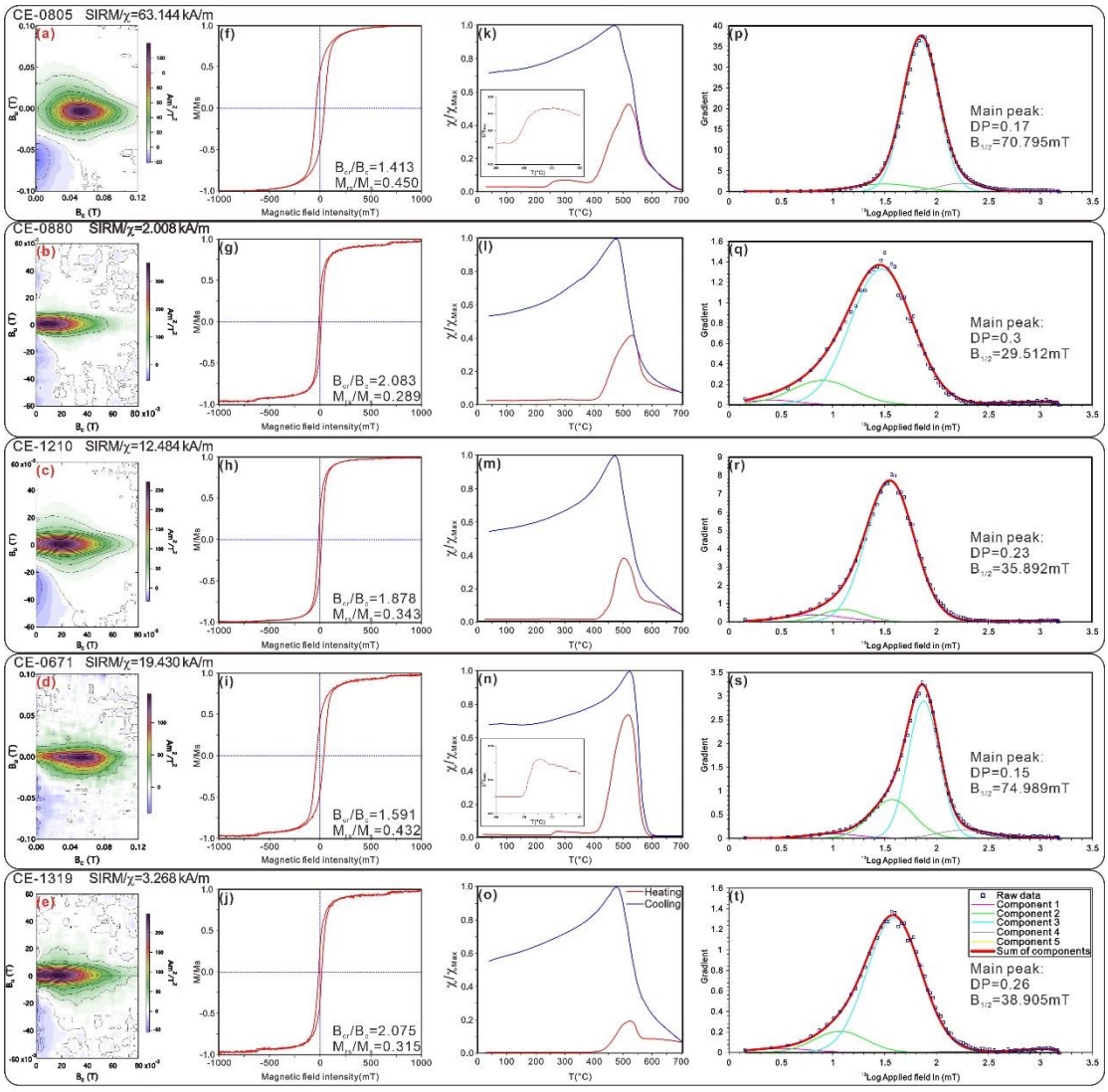

Figure 3. Examples of rock magnetic results of the CE core; for reference the SIRM/χ values of the samples (CE-0805, CE-0880, CE-1210, CE-0671 and CE-1319) are given after the sample number. (a-e) First-order reversal curve (FORC) diagrams. (f-j) Hysteresis loops after paramagnetic slope correction. B_{cr}/B_c and M_{rs}/M_s of the corresponding sample are indicated in the lower right corners. (k-o) Thermomagnetic curves (χ-T curves). Red curves are heating curves, while blue curves are cooling curves. The insets in the lower left corner of panels k and n are enlarged views of the range of 200°C-350°C to better visualize the curves. (p-t) Gradient Acquisition Plot (GAP) of the IRM-CLG Excel workbook. Pink, green, cyan, grey and yellow lines represent five components 1 through 5. Red line is the total fitted curve, and blue squares represent the actually measured IRM gradient values.

3.1.2. Hysteresis loops

The hysteresis loops of the five samples (Fig. 3f-j) can be divided into two types according to their shape. The first type (two samples: CE-0671, CE-0805) is distinctly open, which concurs with higher SIRM/χ values indicative of greigite [*Peters and Dekkers*, 2003]. The M_{rs}/M_s and B_{cr}/B_c ratios of these two samples are close to 0.5 and 1.5, respectively, which points to quasi-SD behavior in agreement the loop shape.

The second type (three samples: CE-0880, CE-1210, and CE-1319) has a narrow shape, with a higher B_{cr}/B_c ratio and a lower M_{rs}/M_s ratio. The main magnetic mineral is magnetite.

3.1.3. χ-T curves

χ-T curves can identify the types of magnetic minerals in the samples [*Duan et al.*, 2017; *Qiang et al.*, 2018]. Two χ-T curve types are distinguished (Fig. 3k-o). The heating curves of the two types show a large decrease at 580 °C, indicating that magnetite is present in the samples and/or is generated during the heating process. The magnetic susceptibility of the first type shows a small rise in at 240 to 260 °C, a rapid and much more prominent rise at 400 °C, and a remarkable peak at 520-540 °C (Fig. 3k-n). It may be that the decomposition of greigite [*Roberts*, 1995; *Roberts et al.*, 2011a; *Torii et al.*, 1996] generates pyrite and pyrrhotite when it was heated to 240-260 °C [*Skinner et al.*, 1964]. On heating to 400 °C, sulfide generated in the previous reaction will gradually convert to magnetite [*Minyuk et al.*, 2013; *Tudryn and Tucholka*, 2004], which will increase the magnetic susceptibility. The second type starts to rise at 400-420 °C and reaches a peak at 500-520 °C (Fig. 3i-o). It may be the coordinated contribution of the Hopkinson effect [*Deng et al.*, 2004; *Minyuk et al.*, 2013] and the transformation of other iron-bearing minerals (greigite, pyrite or siderite) or clay minerals into magnetite during the heating process. This sample type exists widely in the studied core.

3.1.4. IRM-CLG

The results of the IRM-CLG fitting are shown in Fig. 3p-t. In samples CE-0805 and CE-0671, the $B_{1/2}$ values of the main component are located near 70 mT and the DP value is small (< 0.2), which indicates that the dominant magnetic mineral is greigite. In contrast, the $B_{1/2}$ value of main peak is near 30 mT in CE-0880, CE-1210 and CE-1319, while their DP values are notably higher (> 0.2). The main magnetic mineral in these three samples is probably magnetite of detrital origin [*R. Egli*, 2004a; b]. According to the proportion of each peak area, we calculated the IRM contribution of each magnetic mineral in each sample (unit: 10^{-3} Am^2/kg) (Supporting Information S1).

3.2. SEM+EDS

SEM images and EDS results of four selected samples are shown (Fig. 4). The EDS results of CE-0718, CE-0805 and CE-0966 show the presence of iron sulfide (main peaks: iron and sulfur, minor peaks: silicon), while CE-1195 is iron oxide (main peaks: iron and oxygen, minor peaks: silicon and magnesium). Based on the appearance of the element peaks and rock magnetic results, it is determined that the main magnetic mineral of the former is greigite (Fe_3S_4) [*Just et al.*, 2016], and the latter is magnetite (Fe_3O_4). SEM images show that the greigite particles exist in the form of ~10 μm particle framboidal aggregates or 5~10 μm particle aggregates wrapped by silicate cement (red dotted lines in figure 4) [*W Li et al.*, 2019; *Qiang et al.*, 2018]. Greigite will be oxidized if exposed to air [*I Snowball and Thompson*, 1998]. It is possible that

this form of greigite still exists after 20 years storage because the silicate cement prevented it from being completely oxidized in air (or that oxidation is slowed down) [*Jin et al.*, 2011; *Jin et al.*, 2009]. Magnetite particles are in a few μm in size, with a marked angular and octahedral structure and are also wrapped by silicate cement (blue dotted perimeters in figure 4).

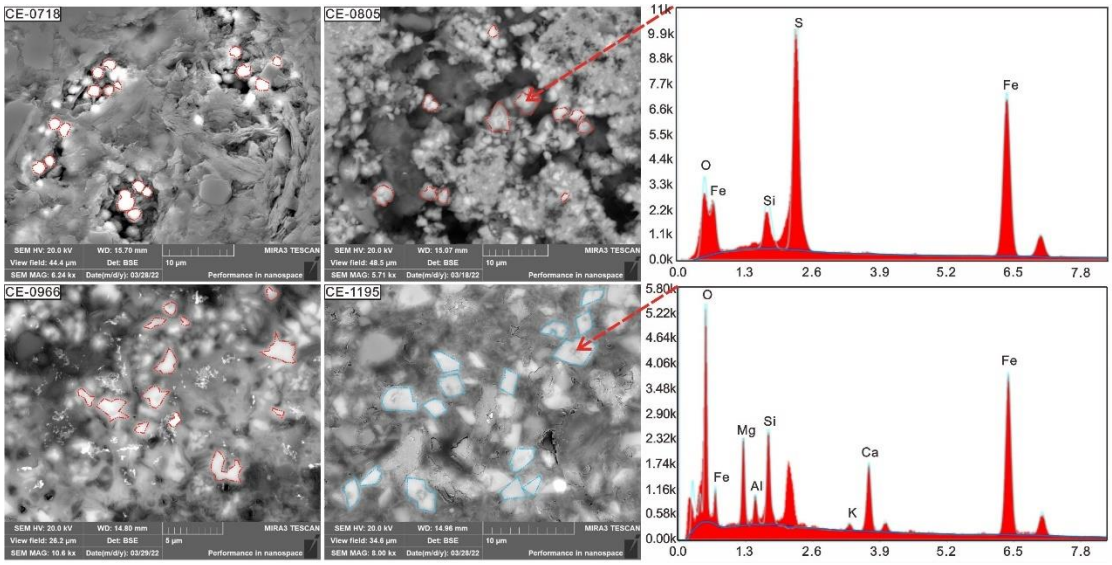

Figure 4. SEM images and EDS results of four selected samples. The main magnetic minerals in CE-0718, CE-0805 and CE-0966 are greigite, while that in CE-1195 is magnetite. The SIRM/χ values of the four samples are 16.374, 63.144, 52.639 and 9.322 kA•m^{-1} respectively.

The rock magnetic data, combined with the SEM images and EDS results, point to magnetite and greigite as the dominant magnetic minerals in the CE core. Magnetite exists widely in the core, while greigite as secondary magnetic mineral is confined to core levels with higher SIRM/χ values. These are typified by light gray clay lithology.

3.3. Greigite quantification

The greigite was quantified in 64 samples with FORC-PCA (Fig. 5). The EM selection is user-defined [*Roberts et al.*, 2018]. The rock magnetic results indicate that the magnetic minerals include SD greigite, SD magnetite and vortex magnetite. Therefore, we set up three EMs in the purple contour region, named EM1, EM2 and EM3, and established a ternary mixtures model. According to the calculated FORC diagrams of three EMs (Fig. 5), we defined EM1 as greigite, EM2 as SD magnetite, and EM3 as vortex magnetite [*Roberts et al.*, 2018]. The absolute contents of the three magnetic minerals in each sample were calculated by the software (Supporting Information S2).

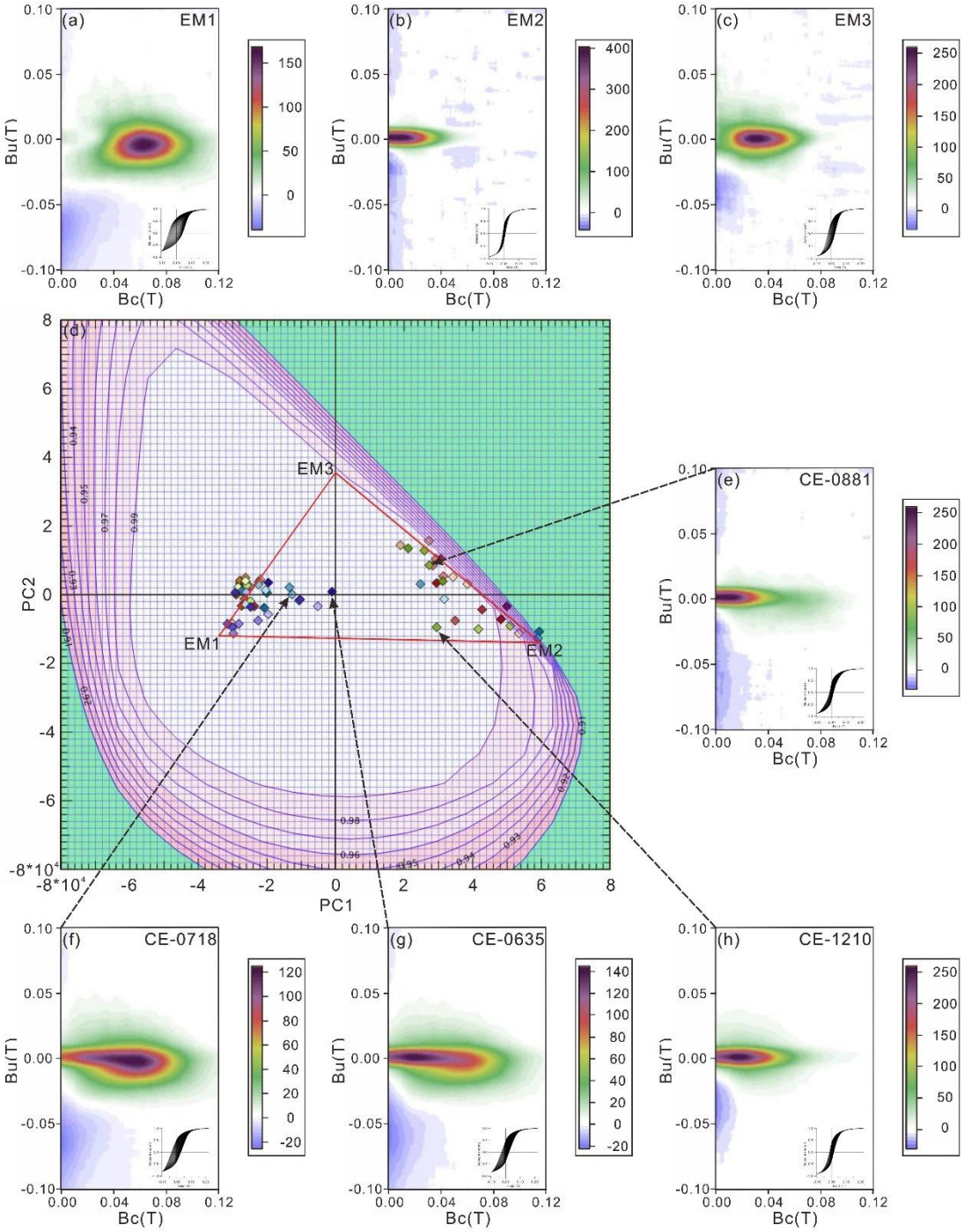

Figure 5. FORC-PCA results of selected samples from the CE core. (a) EM1 represents SD greigite. (b) EM2 represents SD magnetite. (c) EM3 represents vortex magnetite. (d) The triangular mixing space with the positions of the three EMs for 64 samples, the purple outline indicates the space where the FORC distribution begins to become physically unrealistic. (e-h) FORC diagrams of samples CE-0635, CE-0718, CE-0881, and CE-1210 are shown as typical examples. The insets in the lower right corner of panels represent sets of 200 measured FORCs.

FORC-PCA detected 58 samples containing greigite, while IRM-CLG detected 37 samples. The greigite amount in the 37 samples in which greigite was detected by both methods correlates very well (Fig. 6a). The (EM1+EM2+EM3) (absolute)/mass

acquired by FORC-PCA correlates well with the sum of magnetic minerals obtained with IRM-CLG (abbreviated as CLG-SIRM) (Fig. 6c). Evidently, a good linear relationship with Ms/mass of the samples is obtained as well (Fig. 6b). The samples marked with red diamonds are mainly composed of greigite, while the blue samples are magnetite. We multiply the CLG-SIRM with Ms/Mrs to compensate for the grain size dependence and obtained a better linear relationship with (EM1+EM2+EM3) (absolute)/mass than CLG-SIRM (Fig. 6d). Thus, the results of FORC-PCA are meaningful.

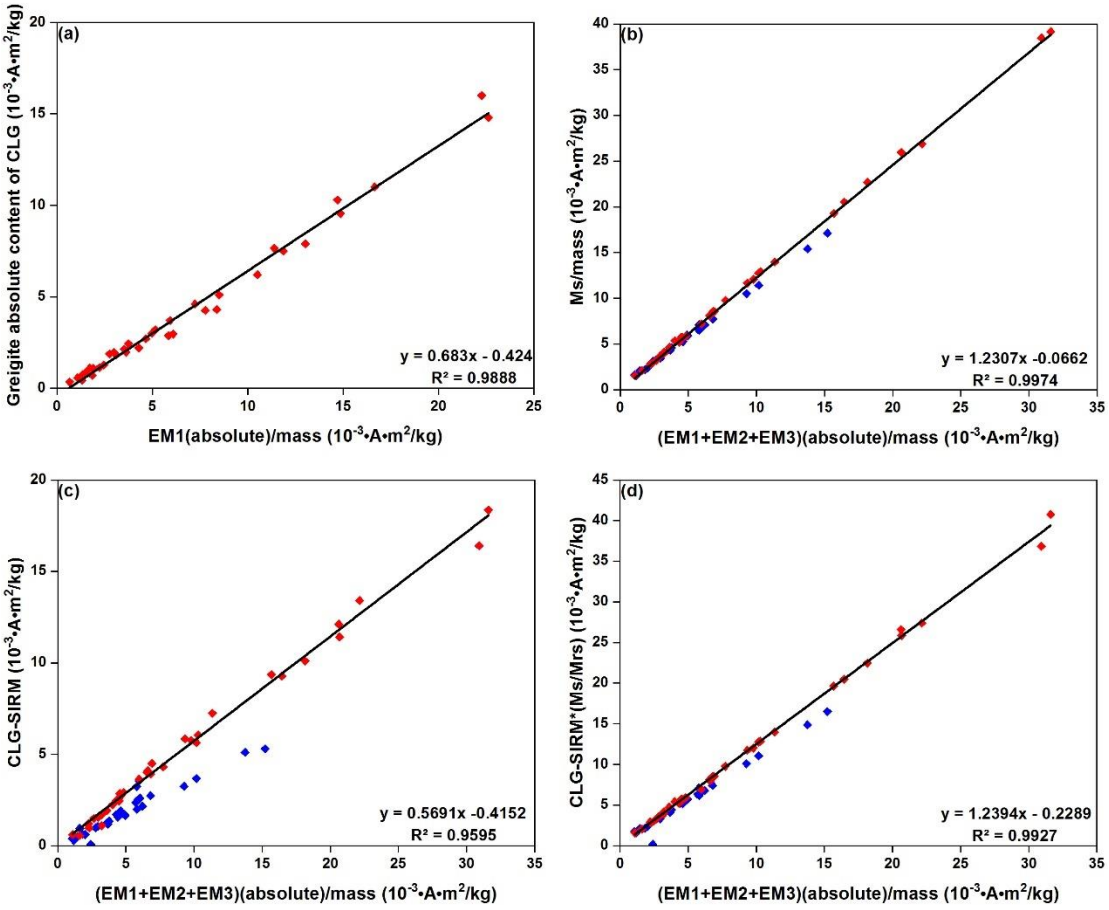

Figure 6. Cross plot of (a) EM1(absolute)/mass and absolute content of greigite of CLG. Cross plots of (EM1+EM2+EM3) (absolute)/mass and Ms/mass (b), CLG-SIRM (c) and CLG-SIRM*(Ms/Mrs) (d). The samples marked with red diamonds are mainly composed of greigite, while the blue samples are magnetite.

4. Discussion

4.1. Quantitative alternative indicator of greigite

The magnetic index IRM_{900mT}/χ is useful to evaluate the relative content of greigite and magnetite [*Larrasoaña et al.*, 2007]. Therefore, we performed correlation analysis between the EM1(absolute)/mass (58 samples) obtained by FORC-PCA and SIRM/χ (Fig. 7). The 37 samples with the greigite content detected by both approaches are indicated with red diamonds, while the 21 samples with greigite only detected by

FORC-PCA are indicated with blue diamonds. The greigite content detection limit of FORC-PCA appears to be lower than that of IRM-CLG, and the presence of greigite is still detected when the value of SIRM/χ is low (Fig. 7).

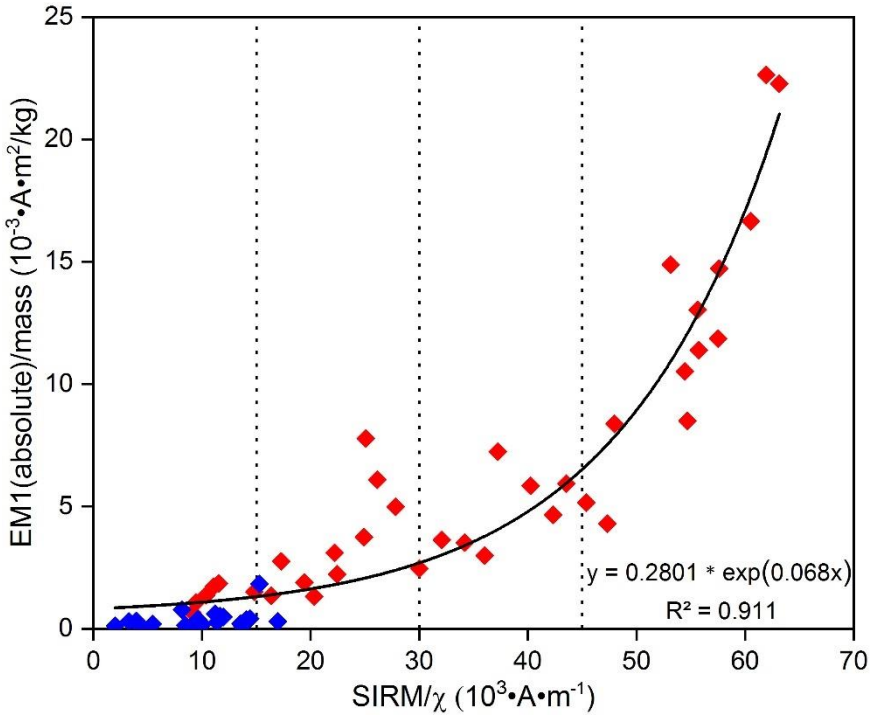

Figure 7. Cross plot of SIRM/χ and EM1(absolute)/mass (58 samples). The 37 samples with the greigite content of detected by FORC-PCA and IRM-CLG are indicated with red diamonds, while the blue diamonds are the 21 samples with greigite only detected by FORC-PCA. The auxiliary dotted lines are to help the visual appreciation of the trend.

We also found that the greigite content and SIRM/χ has an exponential relation: When SIRM/χ < 30 kA·m^{-1}, increasing greigite content comes with a minor SIRM/χ increase. When SIRM/χ > 45kA•m^{-1}, increasing greigite content is marked by notably higher SIRM/χ. Thus, SIRM/χ may be used an indicator of greigite amount, not only its mere presence (Fig. 7). We fitted 37 EM1(absolute)/mass data (red diamonds) with SIRM/χ using an exponential relationship and obtain the equation (Fig. 7). In this way, we can obtain estimates for greigite concentrations from other samples of the CE core.

4.2. Rapid identification method of greigite

Previous studies showed that greigite has a higher SIRM/χ [*Y Fu et al.*, 2008; *Roberts*, 1995], so the SIRM/χ is useful to establish the presence of greigite. The threshold above which greigite is considered to be present differs among the various studies [*W Li et al.*, 2019; *Roberts and Turner*, 1993; *Ron et al.*, 2007; *L. Sagnotti and Winkler*, 1999; *I F Snowball*, 1991]. The differences are in part due to different applied fields used for SIRM acquisition. It is generally believed that the threshold which greigite is present is SIRM/χ > 20 kA·m^{-1}. For the CE core, the samples also appear to contain greigite when SIRM/χ < 10 kA·m^{-1} (Fig. 7). The SIRM/χ value of CE-1195 is 9.322 kA•m^{-1}, and we observed that greigite is suspected to exist in

CE-1195 with SEM. EDS results show high S and Fe peaks, which is helpful to prove the presence of iron sulfide (Fig. 8). Hence, establishing the presence of greigite should not only be based on a SIRM/χ cut-off number, especially when SIRM/χ is low.

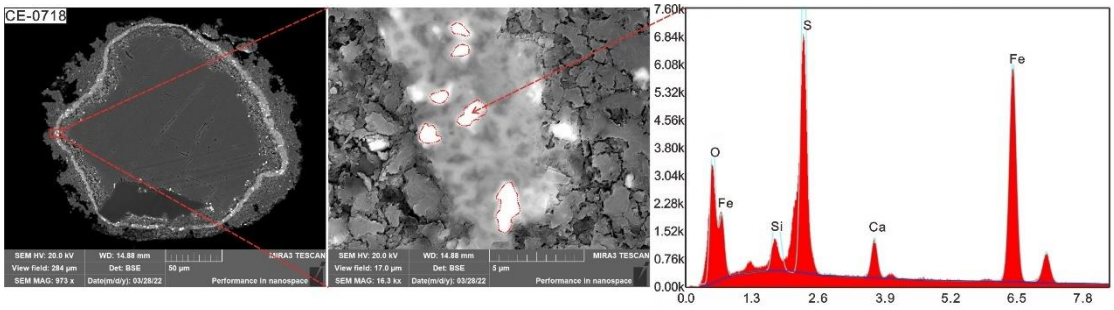

Figure 8. A single mineral SEM image (left) and partially enlarged image (middle) of CE-1195. EDS results (right) show prominent S and Fe peaks.

Next, we evaluate possible correlation between the absolute content of greigite (58 samples) obtained by FORC-PCA and four environmental magnetic indexes, including χ, SIRM, χ_{ARM} and χ_{ARM}/SIRM (Fig. 9). The samples in the red rectangle have greigite as the main magnetic mineral, while the samples in the blue rectangle are magnetite-dominated (Fig. 9). An increasing amount of greigite will lead to magnetic enhancement (Fig. 9a), as also noted in other studies of greigite-bearing sediments [*Reinholdsson et al.*, 2013; *Roberts et al.*, 1999; *Rowan et al.*, 2009]. In comparison with magnetite, a higher greigite amount leads to a marked increase of SIRM (Fig. 9b) and only a slight increase of χ_{ARM} (Fig. 9c). An explanation for this observation is that greigite exists in the form of particle aggregates or is wrapped by silicate cement as observed under SEM (Fig. 4), which produces strong interaction among greigite particles and limit the increase of χ_{ARM} [*Jaep*, 1971; *Yamazaki and Ioka*, 1997]. This results a decrease of χ_{ARM}/SIRM ultimately approaching zero [*McNeill and Kirschvink*, 1993; *Naoji Sugiura*, 1979] (Fig. 9d), and makes the meaning of χ_{ARM} and χ_{ARM}/SIRM not always unequivocal. For samples containing greigite, when using magnetic indicators to reconstruct paleoclimate, magnetic mineralogy effects apparently "outcompete" grain size effects that are typically associated with paleoclimate. Therefore, χ_{ARM} and χ_{ARM}/SIRM are less useful as grain size indicator.

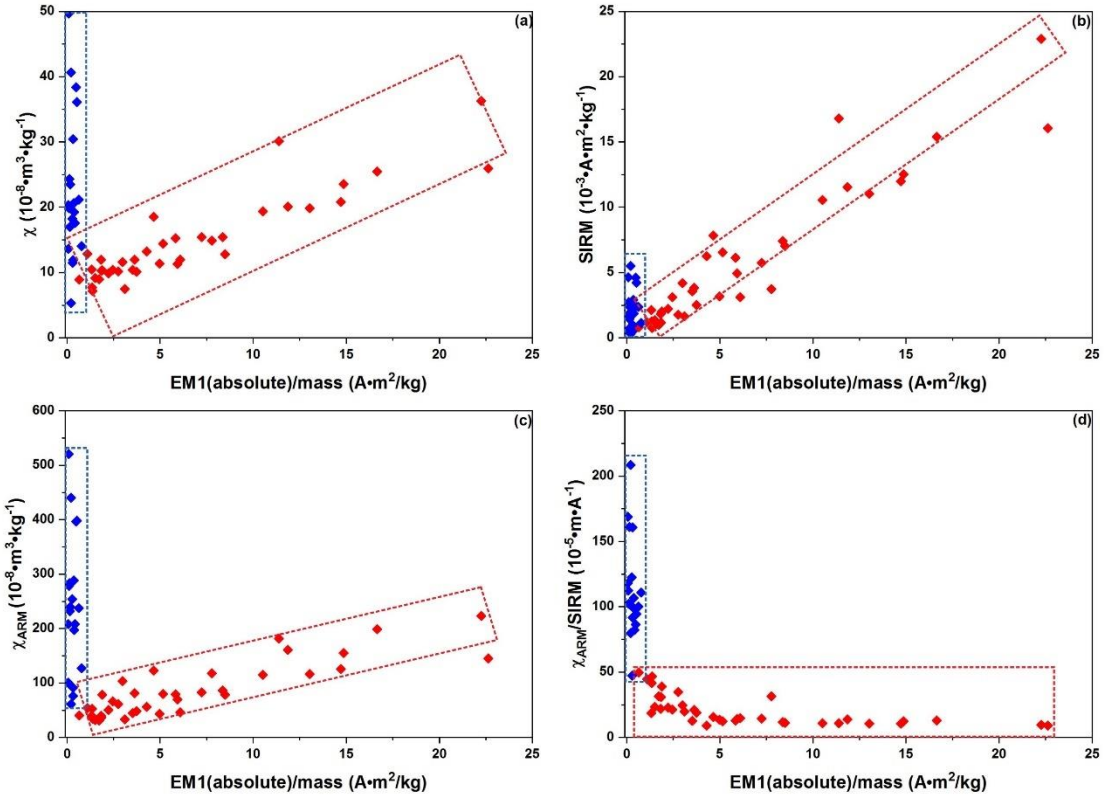

Figure 9. Cross plots of EM1(absolute)/mass versus χ (a), SIRM (b), χ_{ARM} (c) and χ_{ARM}/SIRM (d). The samples in the red rectangle have greigite as the main magnetic mineral, while the samples in the blue rectangle are magnetite dominated.

Based on the above results, we use SIRM/χ as a quantitative greigite indicator for correlation analysis with environmental magnetic indexes χ_{ARM} and χ_{ARM}/SIRM (a total of 1748 samples) (Fig. 10). Red diamonds are the samples with greigite as the main magnetic mineral (37 samples), while blue diamonds are magnetite (21 samples). χ_{ARM} shows two trends with increasing SIRM/χ. For most samples with SIRM/χ values < 15 kA·m^{-1} (the samples in the area delineated with the blue line), χ_{ARM} increases rapidly with only a modest increase of SIRM/χ. For samples with SIRM/χ > 15kA·m^{-1} (and some samples with SIRM/χ < 15 kA·m^{-1}), i.e., the samples in the red enveloped region, χ_{ARM} increases only slowly with increasing SIRM/χ (Fig. 10a). The first group has magnetite as main magnetic mineral, while the second has greigite. Thus, χ_{ARM} is another parameter to evaluate the presence of greigite in the CE core: when χ_{ARM} increases slowly with the increase of SIRM/χ, the sample contains greigite. This method is also applicable to some samples with SIRM/χ<15kA·m^{-1} in the CE core. χ_{ARM}/SIRM decreases gradually and approaches zero with the increase of SIRM/χ (Fig. 10b), which is consistent with the above results (Fig. 9d).

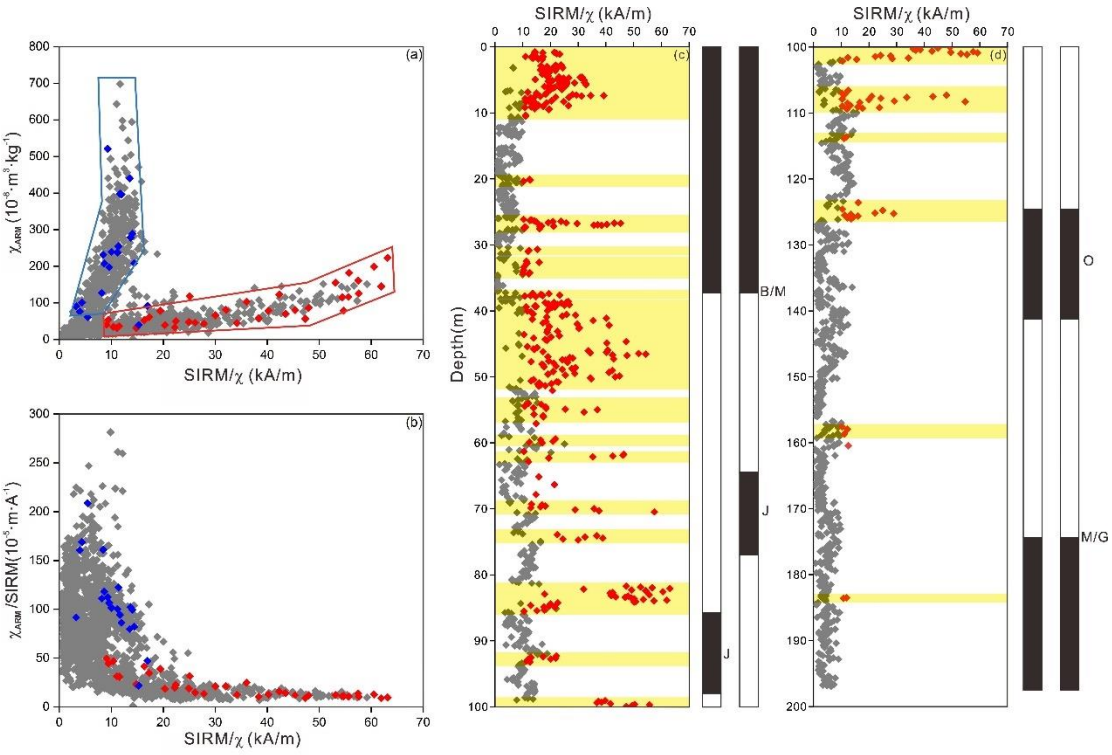

Figure 10. Cross plots of SIRM/χ vs. χ_{ARM} (a), and vs. χ_{ARM}/SIRM (b) of the CE core (a total of 1748 samples). Red diamonds are the 58 samples studied in more detail with greigite as the main magnetic mineral (37 samples), while blue diamonds indicate magnetite-dominated samples (21 samples). The samples in the red enclosed area (panel (a)) point to greigite, while those in the blue region indicate magnetite. (c), (d) are SIRM/χ vs. core depth for the 0-100 m and 100-200 m stratigraphic interval of the CE core. Red diamonds indicate greigite (414 samples). The yellow shaded portions are 20 units containing greigite. Two options for the paleomagnetic polarity are also shown. (B/M: Brunhes/Matuyama boundary, J: Jaramillo subchron, O: Olduvai subchron, M/G: Matuyama/Gauss boundary).

According to the approach outlined in the foregoing, the samples within the red envelope indicate greigite, and the samples in blue envelope are magnetite (Fig. 10a). We finally opted for SIRM/χ > 10 kA·m^{-1} as lower cut-off value to indicate greigite, because it is difficult to distinguish the greigite-bearing samples with SIRM/χ < 10 kA·m^{-1} from magnetite. According to this approach 414 samples contain greigite and displayed on the SIRM/χ vs. depth plot. They make up 20 layers marked with yellow shading (Fig. 10c-d). Including χ_{ARM} in the analysis results in a lower detection limit for greigite than the traditional SIRM/χ cutoff value. Compared to other rock magnetic methods such as FORC, it is faster and particularly suitable for research with large sample collections. The paleomagnetic chronology of the CE core in the interval 38.2-124.57 m is controversial, and greigite widely occurs in the disputed levels, which may be the cause of the perceived discrepancies.

5. Conclusions

We conducted a detailed magnetic property analysis on samples from the CE core,

combined with SEM and X-ray EDS analysis. Our conclusions are listed next: (1) The magnetic minerals in the CE core are magnetite and greigite. Magnetite occurs widely in the CE core as the main magnetic mineral, while greigite as secondary magnetic mineral is confined to the levels with higher SIRM/χ (> 10 kAm^{-1}), with light gray clay as main lithology; (2) FORC-PCA and IRM-CLG as greigite quantification methods show a good correlation, which indicates that FORC-PCA seems robust quantifying magnetic minerals in a magnetite-greigite setting; (3) The relationship between SIRM/χ and the greigite amount is an exponential relation: y = 0.2801*exp(0.068X) with y indicating the greigite amount in $Am^2 \cdot kg^{-1}$ and X the SIRM/χ in $kA \cdot m^{-1}$. Thus SIRM/χ has potential to quantify greigite; (4) Greigite exists in the form of framboidal particle aggregates or particles wrapped by silicate cement which will produce strong interaction among greigite particles and limit the increase of χ_{ARM}. This makes χ_{ARM} another proxy to determine whether greigite occurs in the CE core: when the increase of χ_{ARM} is marginal in comparison with the SIRM/χ increase, greigite is dominant in the sample. This approach is also applicable to samples with low SIRM/χ, below $15kA \cdot m^{-1}$. This method senses greigite quicker than more traditional approaches for greigite detection; compared to rock magnetic methods such as FORC, it is faster and particularly suitable for research of large sample collections. Here, we identify 414 samples containing greigite in the CE core with this method, with a total of 20 layers. Greigite occurs widely in the levels where the paleomagnetic chronology is being disputed: greigite with its variably protracted NRM acquisition mode may be the cause of the perceived discrepancies.

Acknowledgements

This research was financially supported by the National Natural science Foundation of China (NSFC) (41977379), the project of State Key Laboratory of Isotope Geochemistry, Guangzhou Institute of Geochemistry, Chinese Academy of Sciences (SKLaBIG-ZJ-22-01) and the Second Tibetan Plateau Scientific Expedition and Research Program (STEP) (2019QZKK0202). This research used samples provided by the National key Basic Research Program of China (973 Program) (G1998040810). We thank Peng Shasha, Li Wei, Ouyang Tingping, Zhang Lirong, and Lin Yuemin for their help with the experiments.

References

Babinszki, E., E. Márton, P. Márton, & L. Ferenc Kiss (2007), Widespread occurrence of greigite in the sediments of Lake Pannon: Implications for environment and magnetostratigraphy, *Palaeogeography, Palaeoclimatology, Palaeoecology*, *252*(3-4), 626-636. https://doi.org/10.1016/j.palaeo.2007.06.001.

Deng, C., R. Zhu, K. L. Verosub, M. J. Singer, & N. J. Vidic (2004), Mineral magnetic properties of loess/paleosol couplets of the central loess plateau of China over the last 1.2 Myr, *Journal of Geophysical Research: Solid Earth*, *109*(B1), B01103. https://doi.org/10.1029/2003jb002532.

Duan, Z., Q. Liu, C. Gai, & X. Zhao (2017), Magnetostratigraphic and environmental implications of greigite (Fe_3S_4) formation from Hole U1433A of the IODP Expedition 349, South China Sea, *Marine Geology*, *394*, 82-97. https://doi.org/10.1016/j.margeo.2017.02.008.

Egli, R. (2004a), Characterization of Individual Rock Magnetic Components by Analysis of Remanence Curves, 1. Unmixing Natural Sediments, *Studia Geophysica et Geodaetica*, *48*(2), 391-446. https://doi.org/10.1023/B:SGEG.0000020839.45304.6d.

Egli, R. (2004b), Characterization of individual rock magnetic components by analysis of remanence curves. 3. Bacterial magnetite and natural processes in lakes, *Physics and Chemistry of the Earth, Parts A/B/C*, *29*(13-14), 869-884. https://doi.org/10.1016/j.pce.2004.03.010.

Egli, R., A. P. Chen, M. Winklhofer, K. P. Kodama, & C.-S. Horng (2010), Detection of noninteracting single domain particles using first-order reversal curve diagrams, *Geochemistry, Geophysics, Geosystems*, *11*(1), Q01Z11. https://doi.org/10.1029/2009gc002916.

Florindo, F., S. M. Bohaty, P. S. Erwin, C. Richter, A. P. Roberts, P. A. Whalen, & J. M. Whitehead (2003), Magnetobiostratigraphic chronology and palaeoenvironmental history of Cenozoic sequences from ODP sites 1165 and 1166, Prydz Bay, Antarctica, *Palaeogeography, Palaeoclimatology, Palaeoecology*, *198*(1-2), 69-100. https://doi.org/10.1016/s0031-0182(03)00395-x.

Florindo, F., D. Karner, F. Marra, P. Renne, A. Roberts, & R. Weaver (2007), Radioisotopic age constraints for Glacial Terminations IX and VII from aggradational sections of the Tiber River delta in Rome, Italy, *Earth and Planetary Science Letters*, *256*(1-2), 61-80. https://doi.org/10.1016/j.epsl.2007.01.014.

Frank, U., N. R. Nowaczyk, & J. F. W. Negendank (2007), Palaeomagnetism of greigite bearing sediments from the Dead Sea, Israel, *Geophysical Journal International*, *168*(3), 904-920. https://doi.org/10.1111/j.1365-246X.2006.03263.x.

Fu, C., J. Bloemendal, X. Qiang, M. J. Hill, & Z. An (2015), Occurrence of greigite in the Pliocene sediments of Lake Qinghai, China, and its paleoenvironmental and paleomagnetic implications, *Geochemistry, Geophysics, Geosystems*, *16*(5), 1293-1306. https://doi.org/10.1002/2014gc005677.

Fu, Y., T. von Dobeneck, C. Franke, D. Heslop, & S. Kasten (2008), Rock magnetic identification and geochemical process models of greigite formation in Quaternary marine sediments from the Gulf of Mexico (IODP Hole U1319A), *Earth and Planetary Science Letters*, *275*(3-4), 233-245. https://doi.org/10.1016/j.epsl.2008.07.034.

Harrison, R. J., & J. M. Feinberg (2008), FORCinel: An improved algorithm for calculating first-order reversal curve distributions using locally weighted regression smoothing, *Geochemistry, Geophysics, Geosystems*, *9*(5), Q05016. https://doi.org/10.1029/2008gc001987.

Harrison, R. J., J. Muraszko, D. Heslop, I. Lascu, A. R. Muxworthy, & A. P. Roberts (2018), An Improved Algorithm for Unmixing First-Order Reversal Curve Diagrams Using Principal Component Analysis, *Geochemistry, Geophysics, Geosystems*, *19*(5), 1595-1610. https://doi.org/10.1029/2018gc007511.

Heslop, D. (2015), Numerical strategies for magnetic mineral unmixing, *Earth-Science Reviews*, *150*, 256-284. https://doi.org/10.1016/j.earscirev.2015.07.007.

Heslop, D., M. J. Dekkers, P. P. Kruiver, & I. H. M. Van Oorschot (2002), Analysis of isothermal remanent magnetization acquisition curves using the expectation-maximization algorithm, *Geophysical Journal International*, *148*(1), 58-64. https://doi.org/10.1046/j.0956-540x.2001.01558.x.

Heslop, D., & M. Dillon (2007), Unmixing magnetic remanence curves withouta prioriknowledge, *Geophysical Journal International*, *170*(2), 556-566. https://doi.org/10.1111/j.1365-246X.2007.03432.x.

Heslop, D., A. P. Roberts, & L. Chang (2014), Characterizing magnetofossils from first-order reversal

curve (FORC) central ridge signatures, *Geochemistry, Geophysics, Geosystems*, *15*(6), 2170-2179. https://doi.org/10.1002/2014gc005291.

Hu, S., E. Appel, V. Hoffmann, & W. Schmahl (2002a), Identification of greigite in lake sediments and its magnetic significance, *Science in China Series D: Earth Sciences*, *45*(1), 81-87. https://doi.org/10.1007/BF02879699.

Hu, S., E. Appel, V. Hoffmann, W. W. Schmahl, & S. Wang (1998), Gyromagnetic remanence acquired by greigite (Fe3S4) during static three-axis alternating field demagnetization, *Geophysical Journal International*, *134*(3), 831-842. https://doi.org/10.1046/j.1365-246x.1998.00627.x.

Hu, S., A. Stephenson, & E. Appel (2002b), A study of gyroremanent magnetisation (GRM) and rotational remanent magnetisation (RRM) carried by greigite from lake sediments, *Geophysical Journal International*, *151*(2), 469-474. https://doi.org/10.1046/j.1365-246X.2002.01793.x.

Jaep, W. F. (1971), Role of Interactions in Magnetic Tapes, *Journal of Applied Physics*, *42*(7), 2790-2794. https://doi.org/10.1063/1.1660627.

Jin, Z., M. J. Bickle, H. J. Chapman, J. Yu, Z. An, S. Wang, & M. J. Greaves (2011), Ostracod Mg/Sr/Ca and $^{87}Sr/^{86}Sr$ geochemistry from Tibetan lake sediments: Implications for early to mid-Pleistocene Indian monsoon and catchment weathering, *Boreas*, *40*(2), 320-331. https://doi.org/10.1111/j.1502-3885.2010.00184.x.

Jin, Z., M. J. Bickle, H. J. Chapman, J. Yu, S. Wang, & S. Chen (2009), Early to mid-Pleistocene ostracod $\delta^{18}O$ and $\delta^{13}C$ in the central Tibetan Plateau: Implication for Indian monsoon change, *Palaeogeography, Palaeoclimatology, Palaeoecology*, *280*(3-4), 406-414. https://doi.org/10.1016/j.palaeo.2009.06.028.

Just, J., M. J. Dekkers, T. von Dobeneck, A. van Hoesel, & T. Bickert (2012), Signatures and significance of aeolian, fluvial, bacterial and diagenetic magnetic mineral fractions in Late Quaternary marine sediments off Gambia, NW Africa, *Geochemistry, Geophysics, Geosystems*, *13*(9), Q0AO02. https://doi.org/10.1029/2012gc004146.

Just, J., N. R. Nowaczyk, L. Sagnotti, A. Francke, H. Vogel, J. H. Lacey, & B. Wagner (2016), Environmental control on the occurrence of high-coercivity magnetic minerals and formation of iron sulfides in a 640 ka sediment sequence from Lake Ohrid (Balkans), *Biogeosciences*, *13*(7), 2093-2109. https://doi.org/10.5194/bg-13-2093-2016.

Kruiver, P. P., M. J. Dekkers, & D. Heslop (2001), Quantification of magnetic coercivity components by the analysis of acquisition curves of isothermal remanent magnetisation, *Earth and Planetary Science Letters*, *189*(3-4), 269-276. https://doi.org/10.1016/S0012-821X(01)00367-3.

Larrasoaña, J. C., A. P. Roberts, R. J. Musgrave, E. Gràcia, E. Piñero, M. Vega, & F. Martínez-Ruiz (2007), Diagenetic formation of greigite and pyrrhotite in gas hydrate marine sedimentary systems, *Earth and Planetary Science Letters*, *261*(3-4), 350-366. https://doi.org/10.1016/j.epsl.2007.06.032.

Lascu, I., R. J. Harrison, Y. Li, J. R. Muraszko, J. E. T. Channell, A. M. Piotrowski, & D. A. Hodell (2015), Magnetic unmixing of first-order reversal curve diagrams using principal component analysis, *Geochemistry, Geophysics, Geosystems*, *16*(9), 2900-2915. https://doi.org/10.1002/2015gc005909.

Li, M., et al. (2018), Influence of Sea Level Change and Centennial East Asian Monsoon Variations on Northern South China Sea Sediments Over the Past 36 kyr, *Geochemistry, Geophysics, Geosystems*, *19*(5), 1674-1689. https://doi.org/10.1029/2017GC007321.

Li, W., G. Mu, W. Zhang, Y. Lin, D. Zhang, & H. Song (2019), Formation of greigite (Fe_3S_4) in the sediments of saline lake Lop Nur, northwest China, and its implications for paleo-environmental

change during the last 8400 years, *Journal of Asian Earth Sciences*, *174*, 99-108. https://doi.org/10.1016/j.jseaes.2018.11.021.

Liu, J., et al. (2021), Authigenic Iron Sulfides Indicate Sea-Level Change on the Continental Shelf: An Illustration From the East China Sea, *Journal of Geophysical Research: Solid Earth*, *126*(3), e2020JB021222. https://doi.org/10.1029/2020jb021222.

Liu, Q., A. P. Roberts, J. C. Larrasoaña, S. K. Banerjee, Y. Guyodo, L. Tauxe, & F. Oldfield (2012), Environmental magnetism: Principles and applications, *Reviews of Geophysics*, *50*(4), RG4002. https://doi.org/10.1029/2012rg000393.

McNeill, D. F., & J. L. Kirschvink (1993), Early dolomitization of platform carbonates and the preservation of magnetic polarity, *Journal of Geophysical Research: Solid Earth*, *98*(B5), 7977-7986. https://doi.org/10.1029/93jb00353.

Minyuk, P. S., E. E. Tyukova, T. V. Subbotnikova, A. Y. Kazansky, & A. P. Fedotov (2013), Thermal magnetic susceptibility data on natural iron sulfides of northeastern Russia, *Russian Geology and Geophysics*, *54*(4), 464-474. https://doi.org/10.1016/j.rgg.2013.03.008.

Naoji Sugiura (1979), ARM, TRM and magnetic interactions: Concentration dependence,, *Earth and Planetary Science Letters,*, *42*(3), 451-455. https://doi.org/10.1016/0012-821X(79)90054-2.

Neretin, L. N., M. E. Böttcher, B. B. Jørgensen, I. I. Volkov, H. Lüschen, & K. Hilgenfeldt (2004), Pyritization processes and greigite formation in the advancing sulfidization front in the upper Pleistocene sediments of the Black Sea, *Geochimica et Cosmochimica Acta*, *68*(9), 2081-2093. https://doi.org/10.1016/s0016-7037(03)00450-2.

Peck, J. A., & J. W. King (1996), Magnetofossils in the sediment of Lake Baikal, Siberia, *Earth and Planetary Science Letters*, *140*(1–4), 159-172. https://doi.org/10.1016/0012-821X(96)00027-1

Peck, J. A., J. W. King, S. M. Colman, & V. A. Kravchinsky (1994), A rock-magnetic record from Lake Baikal, Siberia: Evidence for Late Quaternary climate change, *Earth and Planetary Science Letters*, *122*(1-2), 221-238. https://doi.org/10.1016/0012-821X(94)90062-0.

Peters, C., & M. J. Dekkers (2003), Selected room temperature magnetic parameters as a function of mineralogy, concentration and grain size, *Physics and Chemistry of the Earth, Parts A/B/C*, *28*(16-19), 659-667. https://doi.org/10.1016/s1474-7065(03)00120-7.

Porreca, M., M. Mattei, & G. Di Vincenzo (2009), Post-deformational growth of late diagenetic greigite in lacustrine sediments from southern Italy, *Geophysical Research Letters*, *36*(9), L09307. https://doi.org/10.1029/2009gl037350.

Qiang, X., X. Xu, H. Zhao, & C. Fu (2018), Greigite formed in early Pleistocene lacustrine sediments from the Heqing Basin, southwest China, and its paleoenvironmental implications, *Journal of Asian Earth Sciences*, *156*, 256-264. https://doi.org/10.1016/j.jseaes.2018.01.033.

Reinholdsson, M., I. Snowball, L. Zillén, C. Lenz, & D. J. Conley (2013), Magnetic enhancement of Baltic Sea sapropels by greigite magnetofossils, *Earth and Planetary Science Letters*, *366*, 137-150. https://doi.org/10.1016/j.epsl.2013.01.029.

Roberts, A. P. (1995), Magnetic properties of sedimentary greigite (Fe_3S_4), *Earth and Planetary Science Letters*, *134*(3-4), 227-236. https://doi.org/10.1016/0012-821x(95)00131-u

Roberts, A. P., L. Chang, C. J. Rowan, C.-S. Horng, & F. Florindo (2011a), Magnetic properties of sedimentary greigite (Fe_3S_4): An update, *Reviews of Geophysics*, *49*(1), RG1002. https://doi.org/10.1029/2010rg000336.

Roberts, A. P., F. Florindo, J. C. Larrasoaña, M. A. O'Regan, & X. Zhao (2010), Complex polarity pattern at the former Plio–Pleistocene global stratotype section at Vrica (Italy): Remagnetization by

magnetic iron sulphides, *Earth and Planetary Science Letters*, *292*(1-2), 98-111. https://doi.org/10.1016/j.epsl.2010.01.025.

Roberts, A. P., F. Florindo, G. Villa, L. Chang, L. Jovane, S. M. Bohaty, J. C. Larrasoaña, D. Heslop, & J. D. Fitz Gerald (2011b), Magnetotactic bacterial abundance in pelagic marine environments is limited by organic carbon flux and availability of dissolved iron, *Earth and Planetary Science Letters*, *310*(3-4), 441-452. https://doi.org/10.1016/j.epsl.2011.08.011.

Roberts, A. P., Q. Liu, C. J. Rowan, L. Chang, C. Carvallo, J. Torrent, & C.-S. Horng (2006), Characterization of hematite (α-Fe_2O_3), goethite (α-FeOOH), greigite (Fe_3S_4), and pyrrhotite (Fe_7S_8) using first-order reversal curve diagrams, *Journal of Geophysical Research: Solid Earth*, *111*(B12), B12S35. https://doi.org/10.1029/2006jb004715.

Roberts, A. P., C. R. Pike, & K. L. Verosub (2000), First-order reversal curve diagrams: A new tool for characterizing the magnetic properties of natural samples, *Journal of Geophysical Research: Solid Earth*, *105*(B12), 28461-28475. https://doi.org/10.1029/2000jb900326.

Roberts, A. P., J. S. Stoner, & C. Richter (1999), Diagenetic magnetic enhancement of sapropels from the eastern Mediterranean Sea, *Marine Geology*, *153*(1–4), 103-116. https://doi.org/10.1016/S0025-3227(98)00087-5.

Roberts, A. P., & G. M. Turner (1993), Diagenetic formation of ferrimagnetic iron sulphide minerals in rapidly deposited marine sediments, South Island, New Zealand, *Earth and Planetary Science Letters*, *115*(1), 257-273. https://doi.org/10.1016/0012-821X(93)90226-Y.

Roberts, A. P., & R. Weaver (2005), Multiple mechanisms of remagnetization involving sedimentary greigite (Fe_3S_4), *Earth and Planetary Science Letters*, *231*(3-4), 263-277. https://doi.org/10.1016/j.epsl.2004.11.024.

Roberts, A. P., X. Zhao, R. J. Harrison, D. Heslop, A. R. Muxworthy, C. J. Rowan, J. C. Larrasoaña, & F. Florindo (2018), Signatures of Reductive Magnetic Mineral Diagenesis From Unmixing of First-Order Reversal Curves, *Journal of Geophysical Research: Solid Earth*, *123*(6), 4500-4522. https://doi.org/10.1029/2018jb015706.

Robertson, D. J., & D. E. France (1994), Discrimination of remanence-carrying minerals in mixtures, using isothermal remanent magnetisation acquisition curves, *Physics of the Earth and Planetary Interiors*, *82*(3), 223-234. https://doi.org/10.1016/0031-9201(94)90074-4.

Ron, H., N. R. Nowaczyk, U. Frank, M. J. Schwab, R. Naumann, B. Striewski, & A. Agnon (2007), Greigite detected as dominating remanence carrier in Late Pleistocene sediments, Lisan formation, from Lake Kinneret (Sea of Galilee), Israel, *Geophysical Journal International*, *170*(1), 117-131. https://doi.org/10.1111/j.1365-246X.2007.03425.x.

Rowan, C. J., & A. P. Roberts (2006), Magnetite dissolution, diachronous greigite formation, and secondary magnetizations from pyrite oxidation: Unravelling complex magnetizations in Neogene marine sediments from New Zealand, *Earth and Planetary Science Letters*, *241*(1-2), 119-137. https://doi.org/10.1016/j.epsl.2005.10.017.

Rowan, C. J., & A. P. Roberts (2008), Widespread remagnetizations and a new view of Neogene tectonic rotations within the Australia-Pacific plate boundary zone, New Zealand, *Journal of Geophysical Research*, *113*(B3), B03103. https://doi.org/10.1029/2006jb004594.

Rowan, C. J., A. P. Roberts, & T. Broadbent (2009), Reductive diagenesis, magnetite dissolution, greigite growth and paleomagnetic smoothing in marine sediments: A new view, *Earth and Planetary Science Letters*, *277*(1-2), 223-235. https://doi.org/10.1016/j.epsl.2008.10.016.

Sagnotti, L., A. Cascella, N. Ciaranfi, P. Macrì, P. Maiorano, M. Marino, & J. Taddeucci (2010), Rock

magnetism and palaeomagnetism of the Montalbano Jonico section (Italy): evidence for late diagenetic growth of greigite and implications for magnetostratigraphy, *Geophysical Journal International*, *180*(3), 1049-1066. https://doi.org/10.1111/j.1365-246X.2009.04480.x.

Sagnotti, L., A. P. Roberts, R. Weaver, K. L. Verosub, F. Florindo, C. R. Pike, T. Clayton, & G. S. Wilson (2004), Apparent magnetic polarity reversals due to remagnetization resulting from late diagenetic growth of greigite from siderite, *Geophysical Journal International*, *160*(1), 89-100. https://doi.org/10.1111/j.1365-246X.2005.02485.x.

Sagnotti, L., & A. Winkler (1999), Rock magnetism and palaeomagnetism of greigite-bearing mudstones in the Italian peninsula, *Earth and Planetary Science Letters*, *165*(1), 67-80. https://doi.org/10.1016/S0012-821X(98)00248-9.

Shen, J., H. LÜ, S. Wang, S. Chen, X. Yang, Y. Wu, & Z. Zhu (2004), A 2.8 Ma record of environmental evolution and tectonic events inferred from the Cuoe core in the middle of Tibetan Plateau, *Science in China Series D: Earth Sciences*, *47*(11), 1025-1034. https://doi.org/10.1360/03yd0214.

Skinner, B. J., R. C. Erd, & F. S. Grimaldi (1964), Greigite, the Thiospinel of Iron, A New Mineral, *American Mineralogist*, *49*, 543-555.

Snowball, I., & R. Thompson (1998), The occurrence of Greigite in sediments from Loch Lomond, *Journal of Quaternary Science*, *3*(2), 121-125. https://doi.org/10.1002/jqs.3390030203.

Snowball, I. F. (1991), Magnetic hysteresis properties of greigite (Fe_3S_4) and a new occurrence in Holocene sediments from Swedish Lappland, *Physics of the Earth and Planetary Interiors*, *68*(1-2), 32-40. https://doi.org/10.1016/0031-9201(91)90004-2.

Tauxe, L., S. K. Banaerjee, R. F. Bulter, & R. Van der Voo (2010), Essentials of paleomagnetism, *University of California Press, California.*

Torii, M., K. Fukuma, C. S. Horng, & T. Q. Lee (1996), Magnetic discrimination of pyrrhotite- and greigite-bearing sediment samples, *Geophysical Research Letters*, *23*(14), 1813-1816. https://doi.org/10.1029/96gl01626.

Tudryn, A., & P. Tucholka (2004), Magnetic monitoring of thermal alteration for natural pyrite and greigite, *Acta Geophysica Polonica*, *52*(4), 509-520.

Wang, F., W. Zhang, X. Nian, A. P. Roberts, X. Zhao, Y. Shang, C. Ge, & Y. Dong (2020), Magnetic evidence for Yellow River sediment in the late Holocene deposit of the Yangtze River Delta, China, *Marine Geology*, *427*, 106274. https://doi.org/10.1016/j.margeo.2020.106274.

Wu, Y., S. Li, A. Lücke, B. Wünnemann, L. Zhou, P. Reimer, & S. Wang (2010), Lacustrine radiocarbon reservoir ages in Co Ngoin and Zigê Tangco, central Tibetan Plateau, *Quaternary International*, *212*(1), 21-25. https://doi.org/10.1016/j.quaint.2008.12.009.

Yamazaki, T., & N. Ioka (1997), Cautionary note on magnetic grain-size estimation using the ratio of ARM to magnetic susceptibility, *Geophysical Research Letters*, *24*(7), 751-754. https://doi.org/10.1029/97gl00602.

Zhang, R., L. Zhu, Q. Ma, H. Chen, C. Liu, & M. Zubaida (2021), The consecutive lake group water storage variations and their dynamic response to climate change in the central Tibetan Plateau, *Journal of Hydrology*, *601*, 126615. https://doi.org/10.1016/j.jhydrol.2021.126615.